ACS OMEGA

http://pubs.acs.org/journal/acsodf

Article

Novel Fluorescent Probe toward Fe^{3+} Based on Rhodamine 6G Derivatives and Its Bioimaging in Adult Mice, *Caenorhabditis elegans*, and Plant Tissues

Jie Zhang,[⊥] Cui-Bing Bai,[*,⊥] Meng-Yu Chen, Shao-Yun Yue, Yu-Xin Qin, Xin-Yu Liu, Meng-Ya Xu, Qi-Jun Zheng, Lin Zhang, Rui-Qian Li, Rui Qiao,[*] and Chang-Qing Qu[*]

Cite This: *ACS Omega* 2021, 6, 8616−8624

Read Online

ACCESS | Metrics & More | Article Recommendations | Supporting Information

ABSTRACT: A new fluorescent probe **LXY** based on the rhodamine 6G platforms has been designed, synthesized, and characterized, which could recognize Fe^{3+} effectively in HEPES buffer (10 mM, pH = 7.4)/CH_3CN (2:3, v/v). And the distinct color change and the rapid emergence of fluorescence emission at 550 nm achieved "naked eye" detection of Fe^{3+}. The interaction mode between them was achieved by Job's plot, MS, SEM, and X-ray single-crystal diffraction. Importantly, the crystal structures proved that Fe^{3+} could induce the rhodamine moiety transform the closed-cycle form to the open-cycle form. But it is interesting that Fe^{3+} did not appear in the crystal structures. Meanwhile, the limit of detection (LOD) of **LXY** to Fe^{3+} was calculated to be 3.47×10^{-9}. In addition, the RGB experiment, test papers, and silica gel plates all indicated that the probe **LXY** could be used to distinguish Fe^{3+} quantitatively and qualitatively on-site. Moreover, the probe **LXY** has also been successfully applied to Fe^{3+} image in *Caenorhabditis elegans*, adult mice, and plant tissues. Thus, **LXY** was considered to have some potential for application in bioimaging.

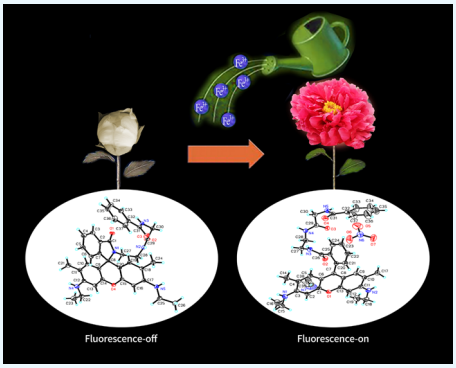

INTRODUCTION

The iron industry is one of the basic industries in all industrialized countries in the world. And Fe^{3+} is one of the most abundant and common metal ions. Fe^{3+} plays an important role in the chemical industry, the environment, and living organisms, especially in the formation of red blood cells, transportation and storage of proteins, and oxygen metabolism.[1−4] However, the accumulation of Fe^{3+} caused by industrial production has resulted in environmental pollution, such as water and soil pollution, which are greatly harmful to the human health.[5,6] In addition, both deficiency and overload of Fe^{3+} can induce various dysfunctions of organisms as well as occurrence of certain diseases.[7−10] Hence, it is important to develop rapid and sensitive methods to determine the distribution of Fe^{3+} to protect the human health and the ecological environment.

In the past few decades, some methods have been developed for the detection of Fe^{3+}, including inductively coupled plasma mass spectrometry (ICP-MS) and atomic absorption spectrometry (ABS). However, their disadvantages including low specificity, complicated sample preparation, and expensive instruments hindered their wide applications.[11−13] Recently, increasingly more attention has been paid to the fluorescence method for the detection of Fe^{3+} because of its ability to detect Fe^{3+} rapidly, sensitively, and selectively. And it could not cause any damage to cell.[14−18] To date, many fluorescent probes for Fe^{3+} have been synthesized successfully, which included coumarin,[19,20] anthracene,[21] BODIPY,[22,23] cyanine,[24] and rhodamines.[25] Among these probes, rhodamine 6G has many advantages over other derivatives, including high extinction coefficients, high quantum yields, excellent photostability, and emission wavelengths.[26−31] However, most rhodamine derivatives were obtained through C═N, but a few compounds linked by amide have been reported.[32−34] It was clear that the amide-modified rhodamine 6G derivatives have more potential coordination sites to bind metal ions than C═N.[35] Moreover, the interaction between rhodamine 6G and metal ions was rarely confirmed by single-crystal structure, which restricted our understanding of its interaction mode between them.[36,37]

In this study, we have designed, synthesized, and characterized the novel fluorescent probe **LXY** based on a rhodamine derivative. It was interesting that the fluorescent probe **LXY** achieved "naked eye" detection of Fe^{3+} in HEPES buffer (10 mM, pH = 7.4)/CH_3CN (2:3, v/v). And other metal ions (K^+, Fe^{2+}, Ca^{2+}, Na^+, Ag^+, Cu^{2+}, Co^{2+}, Mg^{2+}, Cd^{2+}, Ni^{2+}, Ba^{2+}, Pb^{2+}, Al^{3+}, Sr^{2+}, Mn^{2+}, Zn^{2+}, Hg^{2+}, Ce^{3+}, and Y^{3+})

Received: January 25, 2021
Accepted: March 5, 2021
Published: March 18, 2021

https://doi.org/10.1021/acsomega.1c00440
ACS Omega 2021, 6, 8616−8624

Scheme 1. Synthesis (Top) and Crystal Structure (Bottom) of LXY

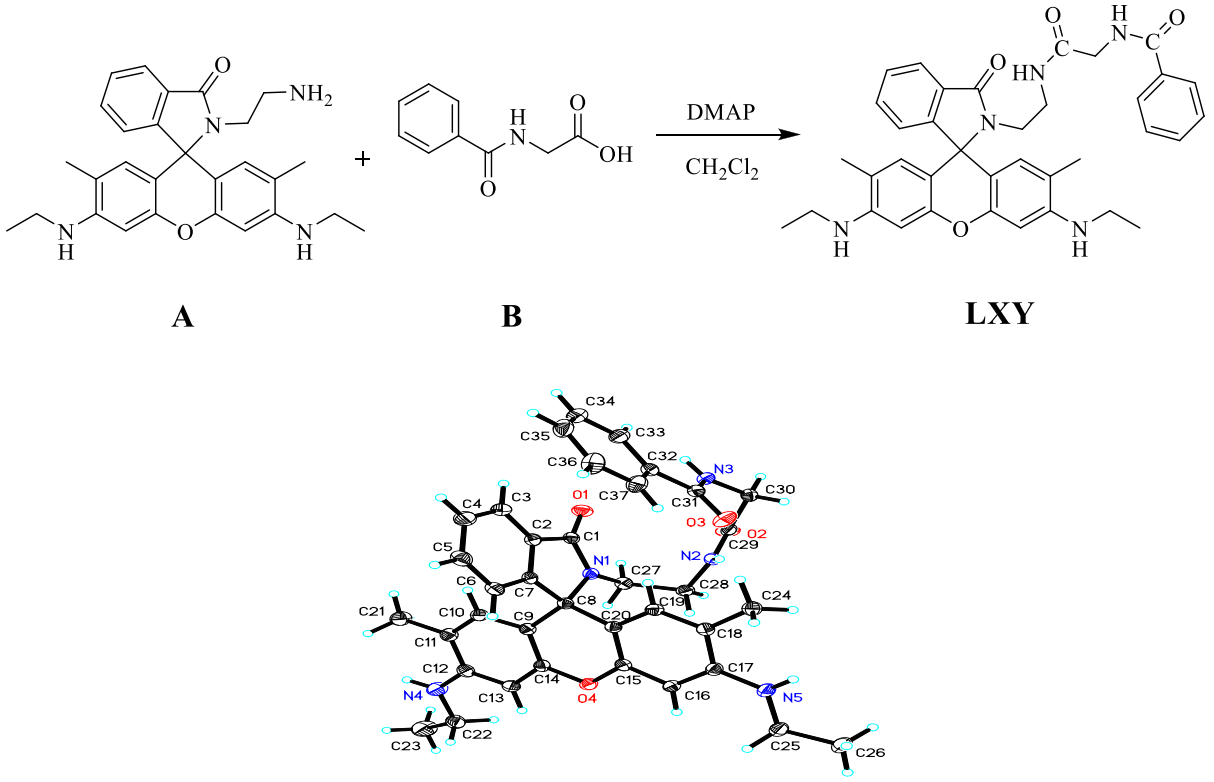

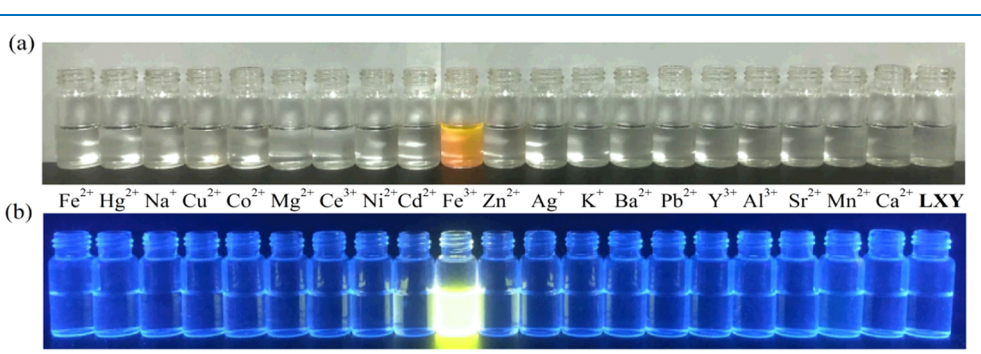

Figure 1. Pictures of **LXY** (10 μM) in HEPES buffer (10 mM, pH = 7.4)/CH_3CN (2:3, v/v) under visible light (a) and UV light (b), mixing with different metal ions (3 equiv).

could not cause any interference. And the LOD of **LXY** to Fe^{3+} is much lower than the WHO and EPA standard (Figure S14).[38−40] In addition, the crystal structures of the open-ring form of **LXY** indicated that only Fe^{3+} could induce the closed lactam ring to open. But Fe^{3+} did not arise in the crystal structure. Furthermore, the RGB experiment conducted on a smartphone and using test papers showed that the probe **LXY** could detect Fe^{3+} in water samples qualitatively and quantitatively. Finally, biological experiments indicated that the probe could achieve fluorescence imaging of Fe^{3+} in *Caenorhabditis elegans*, adult mice, and plant tissues (Scheme 1).

RESULTS AND DISCUSSION

Visual Detection. Initially, the selectivity of probe **LXY** (10 μM) toward various cations was detected by visualizing color change in the solution of HEPES buffer (10 mM, pH = 7.4)/CH_3CN (2:3, v/v). From Figure 1, the solution mixed with Fe^{3+} rather than other cations showed a color change from colorless to pink-red under visible light when the cations were added into the probe of **LXY** solution (Figure 1a). And fluorescence enhancement was observed significantly under UV light (Figure 1b).

Ion Selectivity. Before Fe^{3+} was added, no absorption peaks and emission peaks were observed in the **LXY** solutions from 350 to 600 nm. However, the distinct absorption peak appeared at 515 nm and the strong fluorescence was observed at 550 nm once Fe^{3+} was added (Figure 2). And it is found that other cations did not lead to the spectrum change except Fe^{3+} (Figure S5). Therefore, the detection of **LXY** to Fe^{3+} was not interfered by other metal ions. So, the probe of **LXY** might be used as the selective probe of Fe^{3+}.

Effect of the pH. It is well known that the spirolactam structure in rhodamine 6G could be transformed between the open-ring and closed-ring structures at different pH values. So, the effect of pH on **LXY** toward Fe^{3+} was studied in the solution of HEPES buffer (10 mM, pH = 7.4)/CH_3CN (2:3, v/v) (Figure S6). It is obvious that pH between 6.8 and 8.0 did

https://doi.org/10.1021/acsomega.1c00440
ACS Omega 2021, 6, 8616−8624

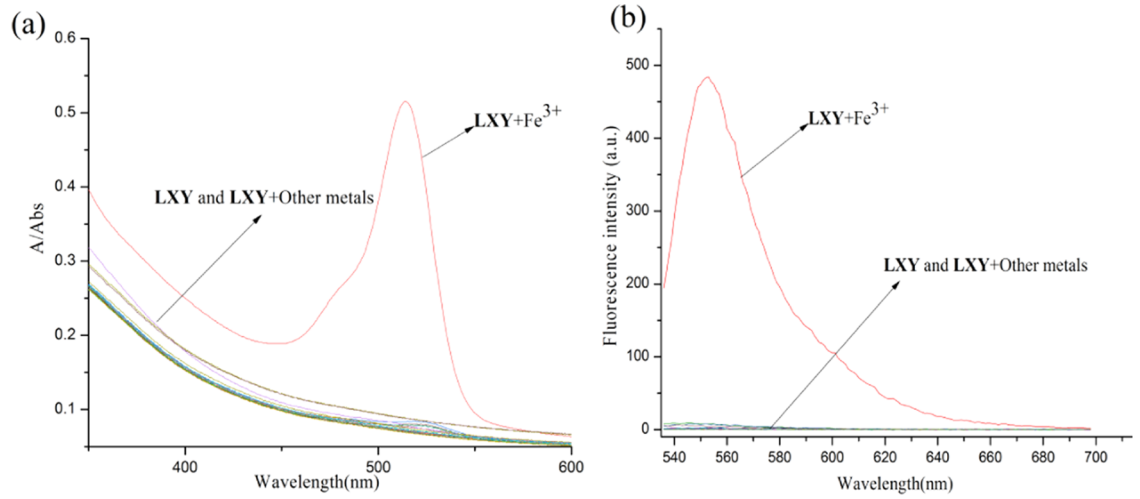

Figure 2. (a) Absorption spectrum of **LXY** (10 μM) in the presence of various metal ions K^+, Na^+, Ag^+, Cu^{2+}, Co^{2+}, Ca^{2+}, Cd^{2+}, Mg^{2+}, Ba^{2+}, Pb^{2+}, Sr^{2+}, Fe^{2+}, Ni^{2+}, Zn^{2+}, Mn^{2+}, Hg^{2+}, Al^{3+}, Y^{3+}, Ce^{3+}, and Fe^{3+} (30 μM) in HEPES buffer (10 mM, pH = 7.4)/CH_3CN (2:3, v/v). (b) Fluorescence spectrum of **LXY** (10 μM) in the presence of various metal ions (30 μM) in HEPES buffer (10 mM, pH = 7.4)/CH_3CN (2:3, v/v), (λ_{ex} = 515 nm).

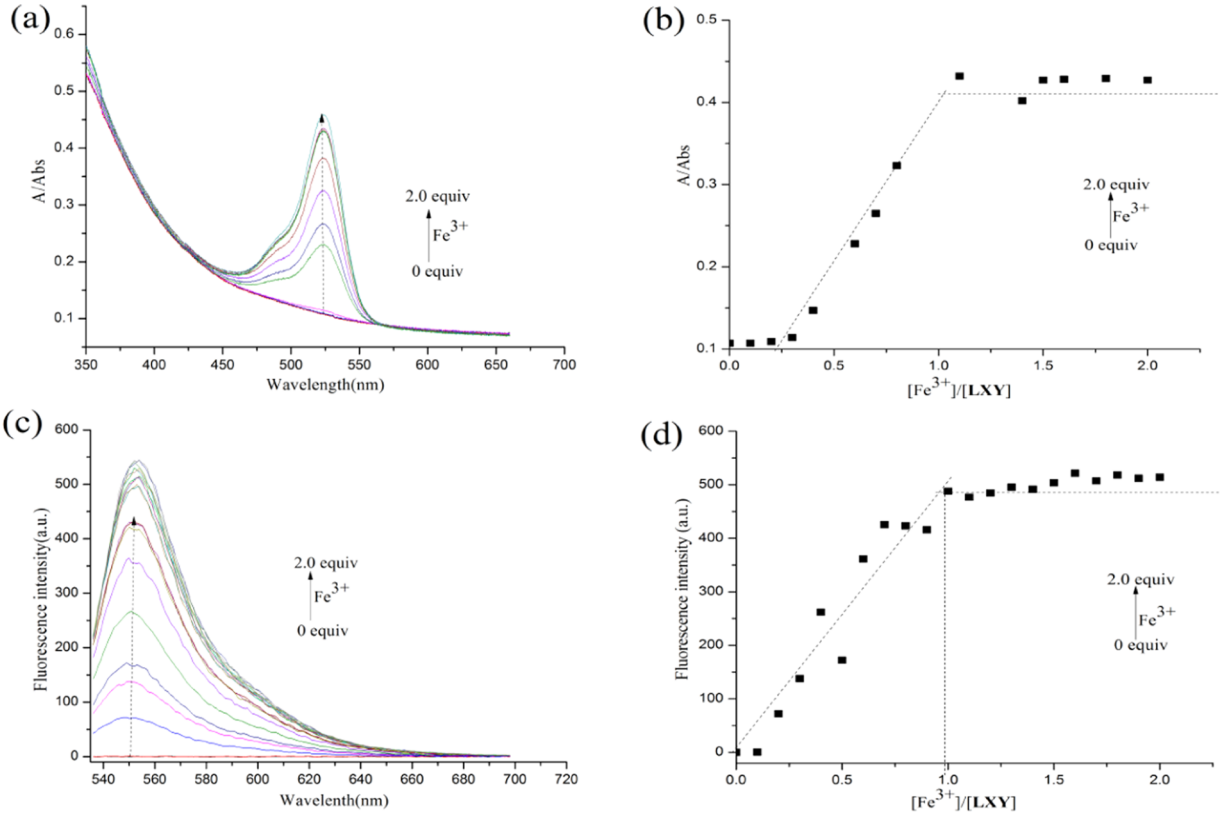

Figure 3. (a, c) Absorption and fluorescence spectra of **LXY** (10 μM) in the presence of different concentrations of Fe^{3+} in solution (λ_{ex} = 515 nm). (b, d) Plots of absorption and fluorescence intensities at 515 and 550 nm with Fe^{3+} concentration in the range of 0.1−2.0 equiv. All measurements were taken in HEPES buffer (10 mM, pH = 7.4)/CH_3CN (2:3, v/v).

not affect the selectivity of **LXY** toward Fe^{3+}. To be close to the pH of the human body, pH = 7.4 was chosen to carry out the living cell imaging.[41]

Sensing Mechanism. To understand the interaction between **LXY** and Fe^{3+}, the mechanism was investigated by Job's plots, MS, X-ray single-crystal diffraction, SEM analysis, and theoretical computations. The stoichiometric ratio of 1:1 between **LXY** and Fe^{3+} was gained by Job's plots (Figures 3b,d and S7). To our surprise, X-ray single-crystal diffraction showed the structure of the probe **LXY** from closed loop to open loop (Scheme 2), which was induced by Fe^{3+}. But Fe^{3+} did not emerge in the single-crystal structures. And the result was also supported by mass spectral analyses because the ion peak was detected at m/z 698.66, which matched [**LXY** + NO_3^- + H_2O]$^+$ well (Figure S8). Moreover, SEM experiment was performed to study the open loop of **LXY** aggregation morphology. After Fe^{3+} (2 equiv) was added into the **LXY** (1 equiv) solution, the morphology of **LXY** changed from

https://doi.org/10.1021/acsomega.1c00440
ACS Omega 2021, 6, 8616−8624

Scheme 2. Interaction between LXY and Fe^{3+}

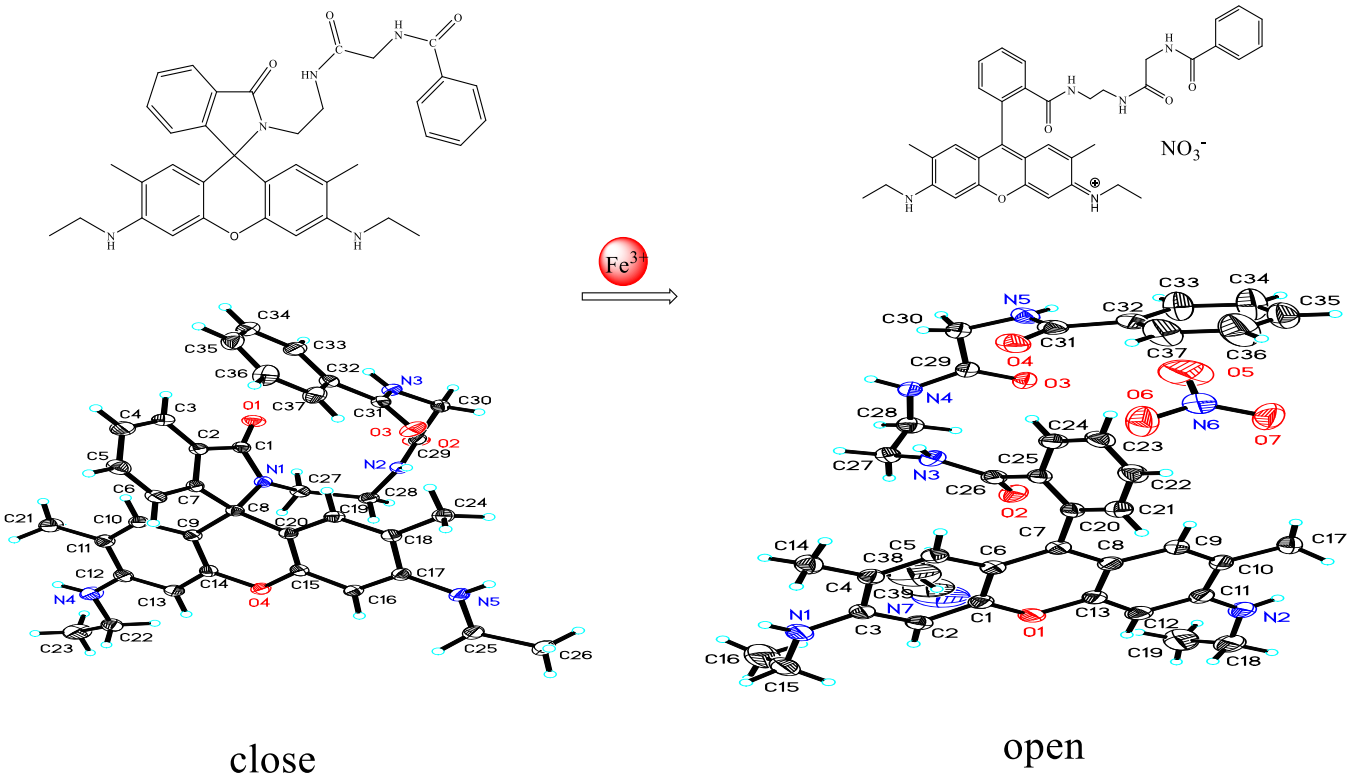

dendritic shape to the porous plane (Figure S9). And the orbital energy and spatial distribution levels of the "open" and "closed" loops were obtained by DFT calculation. It is clear that the electron density for the "closed" loop was mainly distributed mainly over the hippuric acid groups in the highest occupied molecular orbital (HOMO) and the lowest unoccupied molecular orbital (LUMO). However, the electron density for the "open" loop changed obviously after Fe^{3+} was added. The energy gaps of the "open" and "closed" loops were calculated to be 3.6843 and 2.4394 eV, respectively (Figure 4).

Detection of Fe^{3+} by Qualitative and Quantitative Methods. To detect Fe^{3+} in water qualitatively, we prepared test papers. It is interesting that only aqueous solutions of Fe^{3+} caused color changes that could be seen by the "naked eye" (Figure S10). Moreover, the smartphone attracted our attention to detect Fe^{3+} on-site quantitatively.[42] Based on the "naked eye" detection of **LXY**, a color assist APP of smartphone was used to determine the color changes in the RGB (red, green, blue) values and in turn find Fe^{3+} concentration in solution. As shown in Figure 5, a good relationship between the R/B (red/blue) ratio for **LXY** toward Fe^{3+} (R^2 = 0.97805). To verify its accuracy, the experiment was conducted simultaneously by a smartphone and a UV spectrometer. The results showed that the R/B ratio was 2.237, which corresponded to a Fe^{3+} concentration of 23.11 μM, and [Fe^{3+}] was 23.97 μM according to the absorption spectrum (Figure 5a,b). It was found that the error between the two methods was only 3.590%. Hence, it implied that **LXY** could effectively detect Fe^{3+} in water qualitatively and quantitatively.

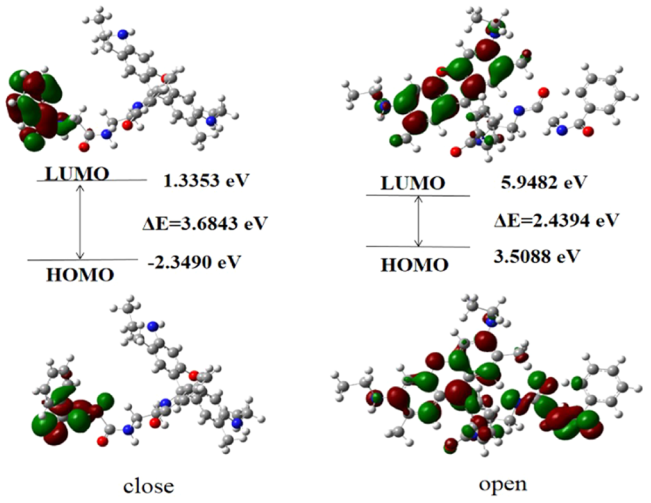

Figure 4. Frontier molecular orbitals of the "closed" and "open" loops.

To further explore the application of the probe **LXY**, the gel plate of **LXY**, which was written using the Fe^{3+} solution, appeared pink-red as detected by the naked eye, while the fluorescence of **LXY** has been enhanced under a 365 UV lamp (Figure S11). The result showed that Fe^{3+} could be qualitatively detected in the solid.

Fluorescence Imaging. We explored the effect of **LXY** on the detection of Fe^{3+} in plant tissues. Figure 6 shows strong green or red fluorescence once Fe^{3+} was added to soybeans treated with **LXY**. And a similar phenomenon was also observed in the root of *Erigeron annuus* (Figure 7). Thus, it is observed that **LXY** had good histocompatibility and could be used for imaging plant tissues.

After the excellent imaging of **LXY** in plant tissues, its imaging in animals was conducted. It is evident that *C. elegans* itself did not show any fluorescence (Figure 8a). While it was incubated with **LXY** (10 μM, DMSO/H_2O = 2:8), weak green

https://doi.org/10.1021/acsomega.1c00440
ACS Omega 2021, 6, 8616−8624

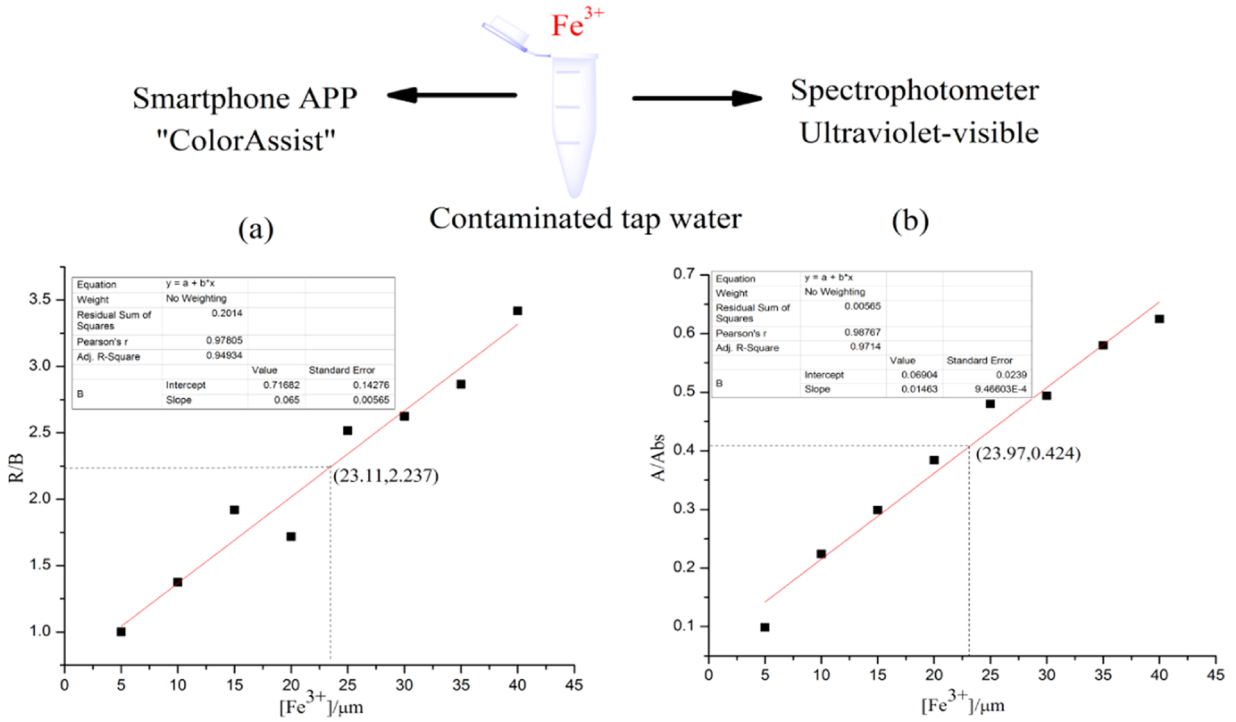

Figure 5. Detection of Fe^{3+} concentration in (a) RGB via a smartphone APP and (b) ABS via a spectrophotometer.

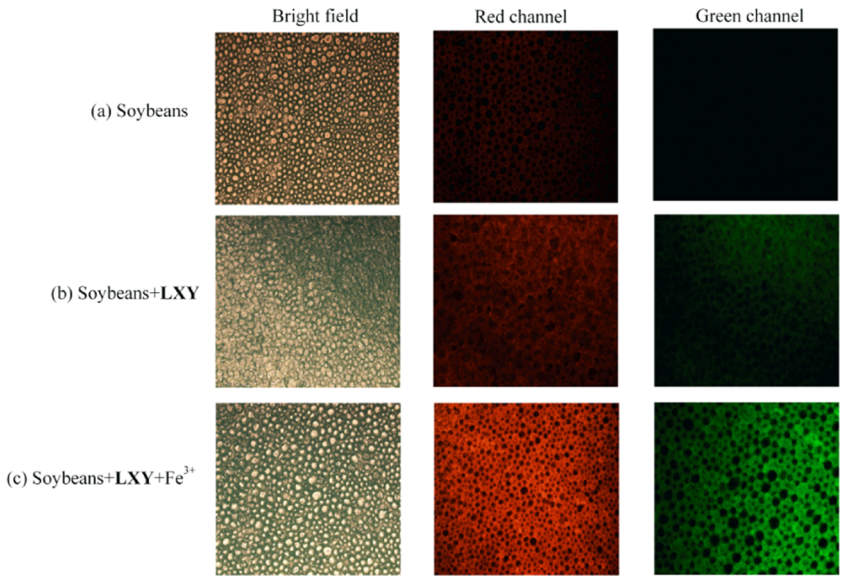

Figure 6. Fluorescence imaging of soybeans. (a) Fluorescence images of soybeans. (b) Fluorescence images of soybeans treated with **LXY** (10 μM, DMSO/H_2O, v/v, 1:1). (c) Fluorescence images of **LXY**-loaded soybeans treated with Fe^{3+} (20 μM, H_2O). From left to right are bright field, red channel (580−650 nm), and green channel (490−550 nm).

fluorescence was observed (Figure 8b). But strong red or green fluorescence emission appeared once Fe^{3+} (20 μM, H_2O) was added and incubated with **LXY** (Figure 8c). After two adult mice were injected with **LXY**, one of them was injected with an aqueous solution containing Fe^{3+} in the same position. It is significant that the fluorescence emerged in the liver, kidney, and heart. But the other did not show any fluorescence in any organs (Figures 9, S12, and S13). The above data confirmed that **LXY** was biocompatible in nature and could be used to test Fe^{3+} ions *in vivo*.

CONCLUSIONS

In summary, the novel **LXY** based on rhodamine 6G was designed, synthesized, and characterized. And **LXY** could distinguish Fe^{3+} from other metal ions effectively in HEPES buffer (10 mM, pH = 7.4)/CH_3CN (2:3, v/v), while the other cations did not cause interference. The recognition mode between **LXY** and Fe^{3+} was confirmed by common methods. However, particularly, single crystals were adopted to ascertain the interaction between them. The probe **LXY** could detect Fe^{3+} in water quantitatively and qualitatively by smartphone and test paper. And it is more interesting that **LXY** could also

https://doi.org/10.1021/acsomega.1c00440
ACS Omega 2021, 6, 8616−8624

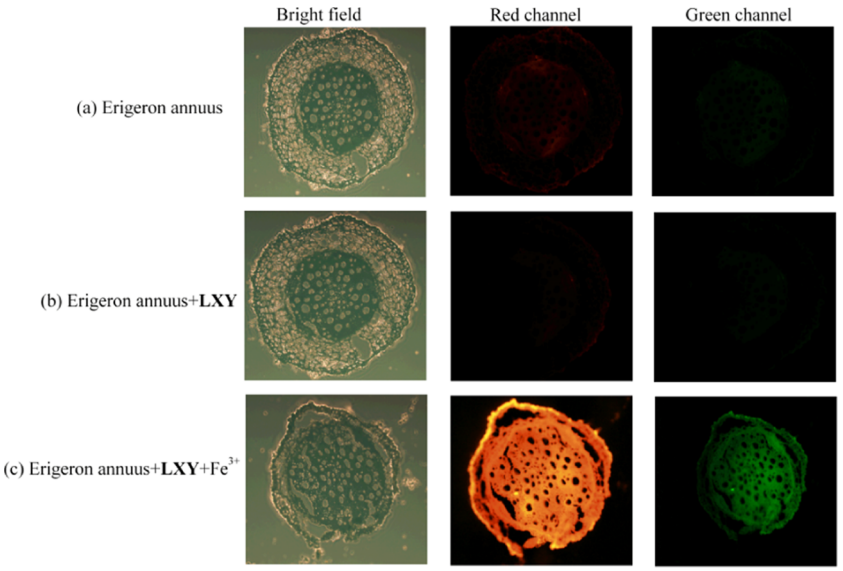

Figure 7. Fluorescence imaging of *Erigeron annuus* root tissues. (a) Fluorescence images of *E. annuus* root tissues. (b) Fluorescence images of *E. annuus* root tissues treated with **LXY** (10 μM, DMSO/H_2O, v/v, 1:1). (c) Fluorescence images of **LXY**-loaded *E. annuus* root tissues treated with Fe^{3+} (20 μM, H_2O). From left to right are bright field, red channel (580−650 nm), and green channel (490−550 nm).

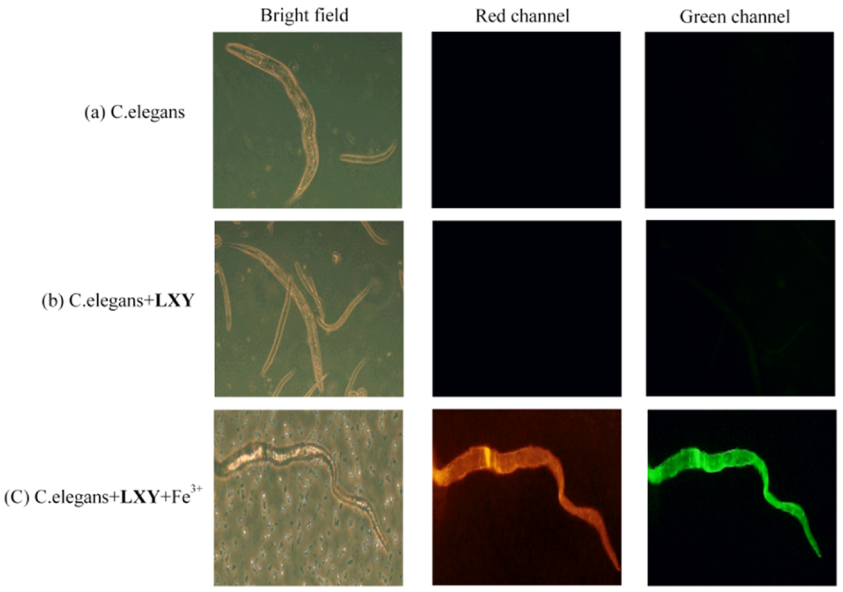

Figure 8. Fluorescence imaging of *C. elegans*. (a) Fluorescence images of *C. elegans*. (b) Fluorescence images of *C. elegans* treated with **LXY** (10 μM, DMSO/H_2O = 2:8). (c) Fluorescence images of **LXY**-loaded *C. elegans* treated with Fe^{3+} (20 μM, H_2O). From left to right are bright field, red channel (580−650 nm), and green channel (490−550 nm).

be used to detect Fe^{3+} in biological samples such as plant tissues, *C. elegans*, and adult mice. Therefore, this article provided a new way for efficient and rapid detection of Fe^{3+} in the chemical industry.

EXPERIMENTAL SECTION

Materials and Physical Methods. ^1H NMR and ^{13}C NMR spectra were recorded on a Bruker spectrometer at 400 MHz using tetramethylsilane (TMS) as an internal standard (DMSO-d_6 as the solvents). Mass spectrum was recorded on a Shimadzu LCMS-IT/TOF mass spectrometer. UV−vis absorption spectrum was recorded on a Shimadzu UV-1601 spectrophotometer. Fluorescence spectrum was recorded on a HORIBA FLUOROMAX-4-NIR spectrometer. The excitation wavelength is 515 nm, and the excitation slit and emission slit are both 2.5 nm. SEM images were acquired on Carl Zeiss Sigma 500. X-ray crystallographic analysis was done at the X-ray crystallography facility, Shanghai Institute of Organic Chemistry (SIOC), Chinese Academy of Sciences (CAS). Biological imaging was performed on a fluorescence inverted microscope from Research Center of Anti-aging Chinese Herbal Medicine of Anhui Province (Fuyang, China). All measurements were carried out at ambient temperature.

All reagents used were of analytical grade and used without further purification unless otherwise stated. The solution of metal ions was prepared from their nitrate salts of K^+, Fe^{2+}, Ca^{2+}, Na^+, Ag^+, Cu^{2+}, Co^{2+}, Mg^{2+}, Cd^{2+}, Ni^{2+}, Ba^{2+}, Pb^{2+}, Al^{3+}, Sr^{2+}, Mn^{2+}, Zn^{2+}, Hg^{2+}, Ce^{3+}, Y^{3+}, and Fe^{3+}. The ligand **LXY** concentration was kept constant (10 μM). The solution of the probe was prepared (10 mM, pH = 7.4)/CH_3CN (2:3, v/v).

https://doi.org/10.1021/acsomega.1c00440
ACS Omega 2021, 6, 8616−8624

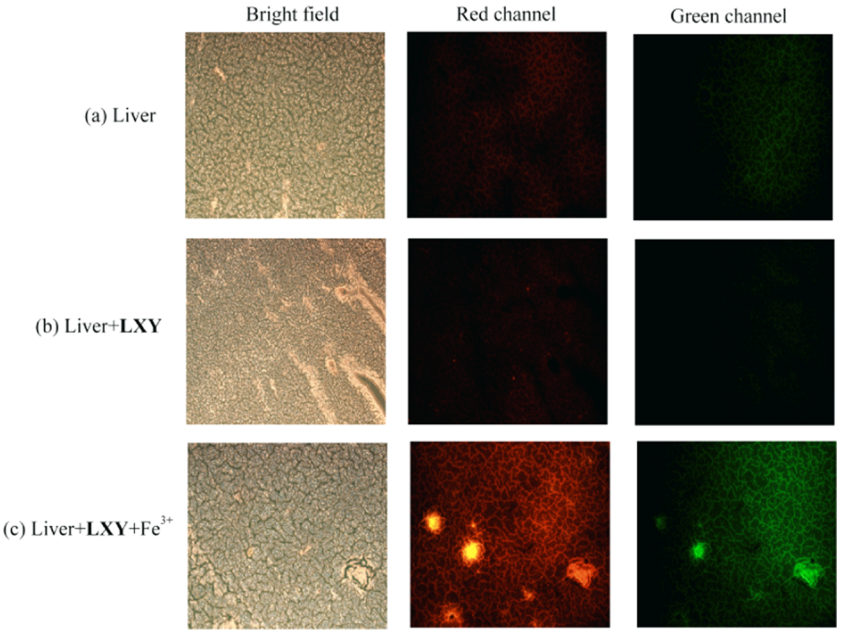

Figure 9. Fluorescence imaging of liver in mice. (a) Fluorescence images of liver without **LXY** and Fe^{3+}. (b) Fluorescence images of liver treated with **LXY** (10 μM, DMSO/H_2O = 2:8). (c) Fluorescence images of **LXY**-loaded liver treated with Fe^{3+} (20 μM, H_2O). From left to right are bright field, red channel (580−650 nm), and green channel (490−550 nm).

SEM samples (**LXY**, **LXY** after Fe^{3+} was added) were dissolved in acetonitrile, and the solution was evaporated and dried at room temperature on a silicone sheet surface. Then, they were tested followed by gold plating. Moreover, the detection limit of **LXY** to Fe^{3+} was calculated by the $3\sigma/s$ method.

Preparation of Test Papers and Silica Gel Plates. Test papers and silica plates were immersed in a solution (100 μM) and desiccated in air at room temperature. The Fe^{3+}, Fe^{2+}, and Hg^{2+} (100 μM) water solutions were used. Test strips were quickly immersed in the prepared solution, distilled water, and tap water. Then, they were dried at room temperature to observe the color change by the "naked eye" and a 365 UV lamp.

Detection of Fe^{3+} by Smartphone (RGB). The **LXY** concentration (10 μM) remained unchanged. And different concentrations of Fe^{3+} were added. The RGB experiment was operated on a smartphone, while UV spectrum was recorded by a spectrophotometer.

Detection of Fe^{3+} in Biological Bodies and Plants. The *in vivo* and plant experiments were conducted with the standard procedure by Research Center of Anti-aging Chinese Herbal Medicine of Anhui Province (Fuyang, China). The specific experimental operation process is given in the Supporting Information.

Crystal Structures of LXY. At room temperature, the probe **LXY** was dissolved in CH_3CN/petroleum ether (1:1) and the probe **LXY** and $Fe(NO_3)_3{\cdot}9H_2O$ (1:1, molar ratio) were dissolved in CH_3CN. After slow evaporation, single crystals, which were suitable for X-ray single-crystal diffraction analysis, were obtained. The crystal data are presented in the Supporting Information. CCDC 2035378 (**LXY**) and 2035380 (open loop of **LXY**) included the supplementary crystallographic data for this paper. These data could be obtained from The Cambridge Crystallographic Data Centre.

Synthesis of the Probe LXY. According to the reported methods, N-(rhodamine 6G) lactam-ethylenediamine (A) was synthesized and purified by recrystallization from ethanol.[43] Then, **A** (460 mg, 1 mmol) and hippuric acid **B** (180 mg, 1 mmol) were dissolved in methylene chloride (25 mL) and also 4-dimethylaminopyridine (DMAP, 122 mg, 1 mmol) was added as a catalyst. The mixture was reacted at room temperature. After the reaction was completed, the solvent was vaporized under vacuum and the crude product was purified by silica gel chromatography (methylene chloride/methanol = 30:1) to get the probe (**LXY**) (Scheme 1). ^{1}H NMR (400 MHz, DMSO-d_6) δ 8.64 (s, 1H), 7.89−7.83 (m, 2H), 7.80 (s, 1H), 7.70 (s, 1H), 7.57−7.44 (m, 5H), 6.95 (s, 1H), 6.26 (s, 2H), 6.13 (d, J = 0.9 Hz, 2H), 5.07 (s, 2H), 3.70 (d, J = 5.8 Hz, 2H), 3.13 (dd, J = 7.2, 5.3 Hz, 6H), 2.78 (dt, J = 9.1, 5.8 Hz, 2H), 1.88 (s, 6H), 1.21 (t, J = 7.1 Hz, 6H). ^{13}C NMR (100 MHz, DMSO-d_6), δ 169.2, 167.9, 166.8, 154.3, 151.3, 148.1, 134.4, 133.1, 131.7, 130.4, 128.6, 128.6, 127.8, 124.0, 122.8, 118.8, 104.8, 96.1, 64.7, 43.1, 37.9, 36.2, 17.4, 14.6 (Figures S2 and S3), MS (ESI) m/z: **LXY** calcd for $C_{38}H_{41}N_5O_3$: 615.32, found 615.58 (Figure S4).

■ ASSOCIATED CONTENT

Supporting Information

The Supporting Information is available free of charge at https://pubs.acs.org/doi/10.1021/acsomega.1c00440.

Synthesis route of N-(rhodamine 6G) lactam-ethylenediamine, ^{1}H NMR and ^{13}C NMR spectra, pH response, competition assays, Job's plot, mass spectroscopy analyses, detection limit, test paper and silica gel, *C. elegans* culture maintenance and fluorescence imaging, bioimaging application in living mice, and X-ray crystallographic data (PDF)

■ AUTHOR INFORMATION

Corresponding Authors

Cui-Bing Bai − *School of Chemistry and Materials Engineering, Fuyang Normal University, Fuyang, Anhui 236037, P. R. China; Key Laboratory of Photochemical*

https://doi.org/10.1021/acsomega.1c00440
ACS Omega 2021, 6, 8616−8624

Conversion and Optoelectronic Materials, TIPC, Chinese Academy of Sciences, Beijing 100190, P. R. China; Research Center of Anti-aging Chinese Herbal Medicine of Anhui Province, Fuyang, Anhui 236037, P. R. China; Email: baicuibing@126.com

Rui Qiao − *School of Chemistry and Materials Engineering, Fuyang Normal University, Fuyang, Anhui 236037, P. R. China; Key Laboratory of Photochemical Conversion and Optoelectronic Materials, TIPC, Chinese Academy of Sciences, Beijing 100190, P. R. China; Research Center of Anti-aging Chinese Herbal Medicine of Anhui Province, Fuyang, Anhui 236037, P. R. China;* orcid.org/0000-0001-5625-0525; Email: qiaorui@fynu.edu.cn

Chang-Qing Qu − *Engineering Research Center of Biomass Conversion and Pollution Prevention Anhui Educational Institutions, Fuyang, Anhui 236037, P. R. China;* Email: qucq518@163.com

Authors

Jie Zhang − *School of Chemistry and Materials Engineering, Fuyang Normal University, Fuyang, Anhui 236037, P. R. China*

Meng-Yu Chen − *School of Chemistry and Materials Engineering, Fuyang Normal University, Fuyang, Anhui 236037, P. R. China*

Shao-Yun Yue − *Engineering Research Center of Biomass Conversion and Pollution Prevention Anhui Educational Institutions, Fuyang, Anhui 236037, P. R. China*

Yu-Xin Qin − *School of Chemistry and Materials Engineering, Fuyang Normal University, Fuyang, Anhui 236037, P. R. China*

Xin-Yu Liu − *School of Chemistry and Materials Engineering, Fuyang Normal University, Fuyang, Anhui 236037, P. R. China*

Meng-Ya Xu − *School of Chemistry and Materials Engineering, Fuyang Normal University, Fuyang, Anhui 236037, P. R. China*

Qi-Jun Zheng − *School of Chemistry and Materials Engineering, Fuyang Normal University, Fuyang, Anhui 236037, P. R. China*

Lin Zhang − *School of Chemistry and Materials Engineering, Fuyang Normal University, Fuyang, Anhui 236037, P. R. China; Research Center of Anti-aging Chinese Herbal Medicine of Anhui Province, Fuyang, Anhui 236037, P. R. China*

Rui-Qian Li − *School of Chemistry and Materials Engineering, Fuyang Normal University, Fuyang, Anhui 236037, P. R. China; Research Center of Anti-aging Chinese Herbal Medicine of Anhui Province, Fuyang, Anhui 236037, P. R. China*

Complete contact information is available at: https://pubs.acs.org/10.1021/acsomega.1c00440

Author Contributions

[⊥]J.Z. and C.-B.B. contributed equally to this work.

Notes

The authors declare no competing financial interest.

■ ACKNOWLEDGMENTS

This work was supported by the National Natural Science Foundation of China (No. 21302019), Anhui Provincial Natural Science Foundation (No. 1908085QB78), the Key Projects of Natural Science Research of Anhui Province Colleges and Universities (No. KJ2019ZD38), Key Program for Young Talents of Fuyang Normal University (No. rcxm201902), Anhui Province Undergraduate Training Programs for Innovation and Entrepreneurship (No. S201910371042), and the Horizontal Cooperation Project of Fuyang Municipal Government and Fuyang Normal University (Nos. XDHX201730 and XDHX201731). This work was also supported by the Open Project Grant of Key Laboratory of Photochemical Conversion and Optoelectronic Materials (PCOM202002), TIPC, Chinese Academy of Sciences.

■ REFERENCES

(1) Guo, Z.; Niu, Q.; Li, T. Highly sensitive oligothiophene-phenylamine-based dual-functional fluorescence ″turn-on″ sensor for rapid and simultaneous detection of Al^{3+} and Fe3+ in environment and food samples. *Spectrochim. Acta, Part A* **2018**, *200*, 76−84.

(2) Liu, J.; Guo, Y.; Dong, B.; Sun, J.; Song, H.; et al. Water-soluble coumarin oligomer based ultra-sensitive iron ion probe and applications. *Sens. Actuators, B* **2020**, *320*, 128361−128372.

(3) Shellaiah, M.; Thirumalaivasan, N.; Aazaad, B.; Awasthi, K.; Ohta, N.; et al. Novel rhodamine probe for colorimetric and fluorescent detection of Fe^{3+} ions in aqueous media with cellular imaging. *Spectrochim. Acta, Part A* **2020**, *242*, 118757−118766.

(4) Zhu, C. C.; Wang, M. J.; Qiu, L.; Hao, S.; Li, K.; Guo, Z.; He, W. A mitochondria-targeting fluorescent Fe^{3+} probe and its application in labile Fe^{3+} monitoring via imaging and flow cytometry. *Dyes Pigm.* **2018**, *157*, 328−333.

(5) Liu, X.; Chen, A.; Wu, Y.; Kan, C.; Xu, J. Fabrication of fluorescent polymer latexes based on rhodamine-B derivatives and their reusable films for Fe^{3+} detection. *Dyes Pigm.* **2020**, *182*, 108633−108641.

(6) Chakraborty, S.; Mandal, M.; Rayalu, S. Detection of iron (III) by chemo and fluoro- sensing technology. *Inorg. Chem. Commun.* **2020**, *121*, 108189−108213.

(7) Chen, J. M.; Zeng, J.; Zhang, Z.; Abulikemu, A. R. A novel colorimetric fluorescent probe for Fe^{3+} based on tetraphenylethylene-rhodamine. *Chin. J. Anal. Chem.* **2019**, *47*, e19139−e19146.

(8) Wu, Z.; Xu, Z.; Tan, H.; Li, X.; Yan, J.; Dong, C.; Zhang, L. Two novel rhodamine-based fluorescent probes for the rapid and sensitive detection of Fe^{3+}: experimental and DFT calculations. *Spectrochim. Acta, Part A* **2019**, *213*, 167−175.

(9) Zhou, F.; Leng, T. H.; Liu, Y. J.; Wang, C. Y.; Shi, P.; Zhu, W. H. Water-soluble rhodamine-based chemosensor for Fe^{3+} with high sensitivity, selectivity and anti-interference capacity and its imaging application in living cells. *Dyes Pigm.* **2017**, *142*, 429−436.

(10) Zhang, W.; Luo, Y.; Zhou, Y.; Liu, M.; Xu, W.; Bian, B.; Tao, Z.; Xiao, X. A highly selective fluorescent chemosensor probe for detection of Fe^{3+} and Ag^{+} based on supramolecular assembly of cucurbit[10]uril with a pyrene derivative. *Dyes Pigm.* **2020**, *176*, 108235−108242.

(11) Zhao, B.; Liu, T.; Fang, Y.; Wang, L. Y.; Kan, W.; Deng, Q. G.; Song, B. A new selective chemosensor based on phenanthro[9,10-d] imidazole-coumarin with sequential "on-off-on" fluorescence response to Fe^{3+} and phosphate anions and its application in live cell. *Sens. Actuators, B* **2017**, *246*, 370−379.

(12) Pang, S.; Liu, S. Y. Dual-emission carbon dots for ratiometric detection of Fe^{3+} ions and acid phosphatase. *Anal. Chim. Acta* **2020**, *1105*, 155−161.

(13) Gao, X. X.; Zhou, X.; Ma, Y. F.; Qian, T.; Wang, C. P.; Chu, F. X. Facile and cost-effective preparation of carbon quantum dots for Fe^{3+} ion and ascorbic acid detection in living cells based on the "on-off-on" fluorescence principle. *Appl. Surf. Sci.* **2019**, *469*, 911−916.

(14) Wang, W.; Wu, M.; Liu, H. M.; Liu, Q. L.; Gao, Y.; Zhao, B. A novel on-off-on fluorescent chemosensor for relay detection of Fe^{3+} and PPi in aqueous solution and living cells. *Tetrahedron Lett.* **2019**, *60*, 1631−1635.

https://doi.org/10.1021/acsomega.1c00440
ACS Omega 2021, 6, 8616−8624

(15) Ghosh, A.; Mandal, S.; Das, S.; Shaw, P.; Chattopadhyay, A.; Sahoo, P. Insights into the phenomenon of acquisition and accumulation of Fe^{3+} in hygrophila spinosa through fluorimetry and fluorescence images. *Tetrahedron Lett.* **2020**, *61*, 151520−151529.
(16) Wang, J.; Jiang, H.; Liu, H. B.; Liang, L.; Tao, J. Pyrene−imidazole conjugate as a fluorescent sensor for the sequential detection of iron(III) and histidine in aqueous solution. *Spectrochim. Acta, Part A* **2019**, *56*, 117725−117731.
(17) Zhang, C.; Gao, R. R.; Wang, H. Y.; Cheng, S. Y.; Xie, A. M.; Dong, W. The synthesis of aggregation-induced emitting vitamin E derivative and its selective fluorescent response toward Fe^{3+}. *Tetrahedron Lett.* **2020**, *61*, 152445−152453.
(18) Tang, W. H.; Tian, Y.; Li, B. P.; Liu, Q. H.; Wang, D. Q.; Jing, X. F.; Zhang, J. J.; Xu, S. Q. Fe^{3+}-selective and sensitive "on-off" fluorescence probe based on the graphitic carbon nitride nanosheets. *Spectrochim. Acta, Part A* **2019**, *210*, 341−347.
(19) Yang, Y. S.; Liang, C.; Yang, C.; Zhang, Y. P.; Wang, B. X.; Liu, J. A novel coumarin-derived acylhydrazone schiff base gelator for synthesis of organogels and identification of Fe^{3+}. *Spectrochim. Acta, Part A* **2020**, *237*, 118391−118398.
(20) Wang, W.; Wu, J.; Liu, Q. L.; Gao, Y.; Liu, H. M.; Zhao, B. 'A highly selective coumarin-based chemosensor for the sequential detection of Fe^{3+} and pyrophosphate and its application in living cell imaging. *Tetrahedron Lett.* **2018**, *59*, 1860−1865.
(21) Pandith, A.; Choi, J. H.; Jung, O. S.; Kim, H. S. A simple and robust PET-based anthracene-appended O−N−O chelate for sequential recognition of Fe^{3+}/CN^- ions in aqueous media and its multimodal applications. *Inorg. Chim. Acta* **2018**, *482*, 669−680.
(22) Shen, B. X.; Qian, Y. Building Rhodamine-BODIPY fluorescent platform using click reaction: naked-eye visible and multi-channel chemodosimeter for detection of Fe^{3+} and Hg^{2+}. *Sens. Actuators, Part B* **2018**, *260*, 666−675.
(23) Sui, B. L.; Tang, S.; Liu, T. H.; Kim, B.; Kevin, D. B. Novel BODIPY-based fluorescence turn-on sensor for Fe^{3+} and its bioimaging application in living cells. *ACS Appl. Mater. Interfaces* **2014**, *6*, 18408−18412.
(24) Zhu, M.; Shi, C.; Xu, X.; Guo, Z.; Zhu, W. Near-infrared cyanine-based sensor for Fe^{3+} with high sensitivity: its intracellular imaging application in colorectal cancer cell. *RSC Adv.* **2016**, *6*, 100759−100764.
(25) Zhang, M.; Shen, C.; Jia, T.; Qiu, J.; Zhu, H.; Gao, Y. One-step synthesis of rhodamine-based Fe^{3+} fluorescent probes via mannich reaction and its application in living cell imaging. *Spectrochim. Acta, Part A* **2020**, *231*, 118105−118112.
(26) Mallick, D.; Bag, B. Altered metal ion selectivity in signalling with heterocyclic tripodal receptor appended rhodamine-B derivatives. *Dyes Pigm.* **2020**, *181*, 108572−108582.
(27) Zhou, F.; Leng, T. H.; Liu, Y. J.; Wang, C. Y.; Shi, P.; Zhu, W. H. Water-soluble rhodamine-based chemosensor for Fe^{3+} with high sensitivity, selectivity and anti-interference capacity and its imaging application in living cells. *Dyes Pigm.* **2017**, *142*, 429−436.
(28) Abebe, F.; Perkins, P.; Shaw, R.; Tadesse, S. A rhodamine-based fluorescent sensor for selective detection of Cu^{2+} in aqueous media: synthesis and spectroscopic properties. *J. Mol. Struct.* **2020**, *1205*, 127594−127602.
(29) Kaur, R.; Saini, S.; Kaur, N.; Singh, N.; Jang, D. O. Rhodamine-based fluorescent probe for sequential detection of Al^{3+} ions and adenosine monophosphate in water. *Spectrochim. Acta, Part A* **2019**, *215*, 117523−117532.
(30) Chen, Q.; Fang, Z. Two sugar-rhodamine "turn-on" fluorescent probes for the selective detection of Fe^{3+}. *Spectrochim. Acta, Part A* **2018**, *193*, 226−234.
(31) Qin, J.; Fu, Z.; Tian, L.; Yang, Z. Study on synthesis and fluorescence property of rhodamine−naphthalene conjugate. *Spectrochim. Acta, Part A* **2019**, *21*, 117854−117868.
(32) Xue, J.; Tian, L.; Yang, Z. A novel rhodamine-chromone schiff-base as turn-on fluorescent probe for the detection of Zn(II) and Fe(III) in different solutions. *J. Photochem. Photobiol., A* **2019**, *369*, 77−84.
(33) Murugan, A. S.; Vidhyalakshmi, N.; Ramesh, U.; Annaraj, J. In vivo bio-imaging studies of highly selective, sensitive rhodamine based fluorescent chemosensor for the detection of Cu^{2+} /Fe^{3+} ions. *Sens. Actuators, B* **2018**, *274*, 22−29.
(34) Wang, Y.; Song, F.; Zhu, J.; Zhang, Y.; Du, L.; Kan, C. Highly selective fluorescent probe based on a rhodamine B and furan-2-carbonyl chloride conjugate for detection of Fe^{3+} in Cells. *Tetrahedron Lett.* **2018**, *59*, 3756−3762.
(35) Qiao, R.; Xiong, W. Z.; Bai, C. B.; Liao, J. X.; Zhang, L. A highly selective fluorescent chemosensor for Fe (III) based on rhodamine 6G dyes derivative. *Supramol. Chem.* **2018**, *30*, 911−917.
(36) Wan, J.; Zhang, K.; Li, C.; Li, Y.; Niu, S. A novel fluorescent chemosensor based on a rhodamine 6G derivative for the detection of Pb^{2+} ion. *Sens. Actuators, B* **2017**, *246*, 696−702.
(37) Kang, H.; Fan, C.; Xu, H.; Liu, G.; Pu, S. A highly selective fluorescence switch for Cu^{2+} and Fe^{3+} based on a new diarylethene with a triazole-linked rhodamine 6G unit. *Tetrahedron* **2018**, *74*, 4390−4399.
(38) WHO*Guidelines for Drinking-Water Quality World Health Organization*; WHO: Geneva, Switzerland, 2011.
(39) Guidelines establishing test procedures for the analysis of pollutants. EPA title 40CFR136 Appendix B: Definition and Procedure for the Determination of the Method Detection Limit (MDL) , 2019.
(40) Dong, S.; Ji, W. M.; Ma, Z. Y.; Zhu, Z. M.; Ding, N.; Nie, J. J.; Du, B. Y. Thermosensitive fluorescent microgels for selective and sensitive detection of Fe^{3+} and Mn^{2+} in aqueous solutions. *ACS Appl. Polym. Mater.* **2020**, *2*, 3621−3631.
(41) Zhang, E. S.; Ju, P.; Li, Q. R.; Hou, X. F.; Yang, H.; Yang, X. J.; Zou, Y.; Zhang, Y. Q. A novel rhodamine 6G-based fluorescent and colorimetric probe for Bi^{3+}: synthesis, selectivity, sensitivity and potential applications. *Sens. Actuators, B* **2018**, *260*, 204−212.
(42) Bai, C. B.; Zhang, J.; Qiao, R.; Zhang, Q. Y.; Mei, M. Y.; Chen, M. Y.; Wei, B.; Wang, C.; Qu, C. Q. Reversible and selective turn-on fluorescent and naked-eye colorimetric sensor to detect cyanide in tap water, food samples, and living systems. *Ind. Eng. Chem. Res.* **2020**, *59*, 8125−8135.
(43) Bai, C. B.; Wang, W. G.; Zhang, J.; Wang, C.; Qiao, R.; Wei, B.; Zhang, L.; Chen, S. S.; Yang, S. A fluorescent and colorimetric chemosensor for Hg^{2+} based on rhodamine 6G with a two-step reaction mechanism. *Front. Chem.* **2020**, *8*, 14−22.

https://doi.org/10.1021/acsomega.1c00440
ACS Omega 2021, 6, 8616−8624